Layer stacking disorder in Mg-Fe chlorites based on powder X-ray diffraction data

Katarzyna Luberda-Durnaś[1,*], Marek Szczerba[1], Małgorzata Lempart[1],
Zuzanna Ciesielska[1], and Arkadiusz Derkowski[1]

[1]Institute of Geological Science, Polish Academy of Science, Senacka 1, 31-002 Krakow

Abstract

The primary aim of this study was the accurate determination of unit-cell parameters and description of disorder in chlorites with semi-random stacking using common X-ray diffraction (XRD) data for bulk powder samples. In the case of ordered chlorite structures, comprehensive crystallographic information can be obtained based on powder XRD data. Problems arise for samples with semi-random stacking, where due to strong broadening of *hkl* peaks with $k \neq 3n$, the determination of unit-cell parameters is demanding. In this study a complete set of information about the stacking sequences in chlorite structures was determined based on XRD pattern simulation, which included determining a fraction of layers shifted by ±1/3**b**, interstratification with different polytypes and 2:1 layer rotations.

A carefully selected series of pure Mg-Fe tri-trioctahedral chlorites with iron content in the range from 0.1 to 3.9 atoms per half formula unit cell was used in the study. In addition, powder XRD patterns were carefully investigated for the broadening of the odd-number basal reflections to determine interstratification of 14 and 7 Å layers. These type of interstratifications were finally not found in any of the samples. This result was also confirmed by the XRD pattern simulations, assuming interstratification with *R*0 ordering.

Based on *h0l* XRD reflections, all the studied chlorites were found to be the IIbb polytype with a monoclinic-shaped unit cell ($\beta \approx 97°$). For three samples, the *hkl* reflections with $k \neq 3n$ were partially resolvable; therefore, a conventional indexing procedure was applied. Two of the chlorites were found to have a monoclinic cell (with $\alpha, \gamma = 90°$). Nevertheless, among all the samples, the more general triclinic (pseudomonoclinic) crystal system with symmetry $C\bar{1}$ was assumed, to calculate unit-cell parameters using Le Bail fitting.

A detailed study of semi-random stacking sequences shows that simple consideration of the proportion of IIb-2 and IIb-4/6 polytypes, assuming equal content of IIb-4 and IIb-6, is not sufficient to fully model the stacking structure in chlorites. Several, more general, possible models were therefore considered. In the first approach, a parameter describing a shift into one of the ±1/3**b** directions (thus, the proportion of IIb-4 and IIb-6 polytypes) was refined. In the second approach, for samples with slightly distinguishable *hkl* reflections with $k \neq 3n$, some kind of segregation of individual polytypes (IIb-2/4/6) was considered. In the third approach, a model with rotations of 2:1 layers about 0°, 120°, 240° was shown to have the lowest number of parameters to be optimized and therefore give the most reliable fits. In all of the studied samples, interstratification of different polytypes was revealed with the fraction of polytypes being different than IIbb ranging from 5 to 19%, as confirmed by fitting of *h0l* XRD reflections.

Keywords: Chlorites, polytype interstratification, stacking disorder, powder X-ray diffraction

Introduction

Interest in the chlorite structure has been growing since it was first described by Pauling (1930), who showed that chlorites are built of two main units: the 2:1 and brucite-type layers, arranged in an alternating manner. The negative charge generated in the 2:1 layer $(R^{2+}, R^{3+})_3(Si_{4-x}Al_x)O_{10}(OH)_2$ is compensated by the octahedral sheet $(R^{2+}, R^{3+}, \square)_3(OH)_6$ present in the interlayer; where R^{2+} is Mg, Fe; R^{3+} is Al, Fe, rarely Cr, Mn; $\square$ is vacancy. In the 2:1 layer, one octahedral sheet is sandwiched between two tetrahedral sheets, thus for one crystallographic unit cell, six octahedral and eight tetrahedral sites are available. In the interlayer, a maximum of six octahedral sites can be occupied. Depending on the occupancy of available octahedral sites, four sub-groups of chlorites can be distinguished (tri-trioctahedral; di-trioctahedral; tri-dioctahedral; di-dioctahedral). Tri-trioctahedral chlorites, where virtually all six octahedral sites (in both the 2:1 layer and interlayer sheets) are occupied by divalent cations, are the most abundant class.

Independently of octahedral occupancy, Brown and Bailey (1962) proposed a chlorite polytype classification based on a mutual arrangement of the interlayer sheet and the 2:1 layer and involving a shift by **a/3** (Ia, IIa, Ib, IIb). These four structural units (2:1 layer + interlayer sheet) can be shifted with respect to each other by ±1/3**b**. The shift results in aperiodic stacking—a so-called

semi-random structure—manifesting in diffuse *hkl* reflections with $k \neq 3n$ due to incoherent scattering (Brindley et al. 1950).

For regular-stacking chlorites, 12 unique periodic arrangements of 2:1 layers (with respect to the position of the adjacent 2:1 layer) occur, resulting in 12 polytypes with different cell-shapes and symmetries. In the case of semi-random stacking structures, they are reduced to six arrangements based on two types of unit-cell shapes: (1) orthorhombic-shaped with $\alpha = \beta = \gamma = 90°$, and (2) monoclinic-shaped with $\beta \approx 97°$. In X-ray diffraction (XRD) patterns, an identification of polytypes as well as the unit-cell shape can be performed based on *h0l* reflections, even for samples with semi-random stacking (Brown and Bailey 1962).

To differentiate between polytypes with the same structural units and the same unit-cell shape, for example, IIb-2, IIb-4, and IIb-6, which differ by the position of subsequent interlayer sheets sandwiching the 2:1 layer, accurate information about *hkl* intensities is needed. Based on powder diffraction patterns, finding the symmetry of such polytypes and distinguishing between them is not possible even for regular-stacking specimens. For example, in *C2/m*, F(*hkl*), and F(*h̄kl*) are equal; however, in powder diffraction patterns the reflections overlap and individual intensities cannot be distinguished (Aja et al. 2015). This situation becomes more complicated for semi-random stacking structures, characterized by an additional shift of ±1/3**b**.

The polytype IIb-4 is often reported as the most abundant (e.g., Brown and Bailey 1962; Joswig et al. 1980; Zheng and Bailey 1989; Aja et al. 2015; Beaufort et al. 2015). Such an assertion can be supported by records available in crystallographic databases; for example, in the Crystallographic Open Database (COD), 32 trioctahedral chlorite structures were found (Grazulis et al. 2009). Eighteen of the structures become modified under different pressures (Welch and Marshall 2001; Zanazzi et al. 2006, 2007) and temperature conditions (Guggenheim and Zhan 1999; Zanazzi et al. 2009). Another 16 structures belong to untreated, raw chlorites. Among them, two are Ib-1 ($\beta = 90°$) chlorites (Shirozu and Bailey 1965) and one is the $Ia\bar{4}$ polytype (Bailey 1986). Nine IIb structures were found in triclinic (IIb-4) and four in monoclinic (IIb-2) crystal systems. Except for one (Walker and Bish 1992), all deposited structures were refined based on single-crystal X-ray or neutron (Joswig et al. 1980) diffraction data. These data show that despite great progress in powder diffraction in recent decades, especially in the implementation of the Rietveld method, the refinement of a chlorite structure based on powder XRD data is still challenging. In addition, the XRD-based refinement of semi-random stacking chlorites has been tested without obtaining satisfactory fits (Walker and Bish 1992).

An invaluable technique that allows for investigating polytypes and disordered stacking sequences in chlorites is high-resolution transmission electron microscopy (HRTEM). This method is often supported by simulations of powder XRD patterns (Kogure et al. 2006; Kameda et al. 2007) and is to-date the only alternative for the single-crystal diffraction method in studying stacking sequences in chlorites.

This study represents an attempt to refine the stacking patterns of semi-random chlorite structures based only on the simulation of powder XRD data. Here we show that, despite difficulties,

reliable results involving the magnitude of the random shift, 2:1 layers rotations and interstratification of polytypes can be obtained using a simple approach.

SAMPLES

Finding pure chlorite, not interstratified with vermiculite (Herbillion and Makumbi 1975), serpentine (Ahn and Peacor 1985; Ryan and Reynolds 1996; Xu and Veblen 1996; Inoue and Kogure 2016), or kaolinite (Hillier and Velde 1997) is challenging, especially for Fe-rich chlorites. Therefore, a large set of chlorites was pre-tested to select the purest chlorite material for further analyses.

Seven tri-trioctahedral chlorites from a common Mg-Fe-series were used in the study. Sptb (from Spitsbergen, Norway), SG7 (Strzegom, Poland), and MtBl (Plan de l'Aguille, Massif du Mont-Blanc, France) were gently ground in a mortar to pass through a <100 μm sieve; POST, CCC, CCa-2 (all three from Flagstaff Hill, El Dorado County, California, U.S.A.; Source: Clay Project of the Clay Minerals Society, Post and Plummer 1972) and Mal (Malacachetta, Brazil) were ground with hexane in a McCrone micronizing mill for 5 min. MtBl, Sptb, and CCC chlorites were characterized in the work of Lempart et al. (2018). An identical preparation procedure for all the samples was not possible because some samples were obtained thanks to the courtesy of collaborating laboratories and in a few cases, these were received after grinding.

METHODS

Chemical composition

Chemical analyses of chlorites were performed using electron microprobe analysis (EMPA) with a JEOLJXA-8230 microprobe. Grains with a 50–100 μm diameter were fixed in an epoxy resin and polished with a diamond paste to about half their thickness; powder samples were prepared with randomly oriented crystallites. Individual crystals of chlorites were analyzed in the wavelength-dispersion spectroscopy (WDS) mode with an accelerating voltage of 15 kV, probe current of 15 nA, and a beam diameter of 3–5 μm. The counting time was 20 s for the peak and 10 s for both background positions. A high homogeneity of chemical composition among chlorite crystals was found during observations using high-contrast backscattered electron (BSE) images. For each chlorite sample, 25 measurement points were found to be sufficient to obtain a reliable and repeatable analysis. Structural formulas (per formula unit) were calculated based on 14 oxygen atoms.

The Fe(II)/Fe(III) ratio of the natural samples studied was determined via Mössbauer transmission measurements using an MsAa-3 spectrometer. For a 14.41-keV resonant transition in ^{57}Fe a single line commercial $^{57}Co(Rh)$ source kept at room temperature was applied. Collection of data lasted about 24 h for each spectrum at room temperature. The Fe(II)/Fe(III) ratio was calculated using transmission integral approximation. Spectral shifts were reported vs. natural α-Fe at room temperature.

Structural analysis

To minimize the effects of texture and preferred orientation in XRD, capillary measurements (diameter: 0.3 mm) were performed. Bruker D8 Advance diffractometer (Karlsruhe, Germany) in Debye-Scherrer geometry with a CoKα X-ray tube (35 kV, 40 mA) was used. The X-ray beam was monochromatized and formed using a Göbel mirror, 0.2 mm fixed slit, 2.5° Soller slits, and a beam knife. For the secondary beam, a VANTEC detector equipped with radial and 2.5° Soller slits was used. The scan range was set from 5 to 110° 2θ with a step size of 0.007°. Qualitative analyses were performed using DIFFRAC.EVA software version 4.2.0.31 equipped with a Crystallographic Open Database (COD) (Grazulis et al. 2009). Unit-cell parameter determination was performed using TOPAS software, ver. 5, with the indexing algorithm based on iterative use of least-squares fitting, following Coelho (2003).

A simulation of XRD patterns was performed using Sybilla3D and 2D software (Chevron ETC proprietary). Parameters describing: (1) the content of the IIb-2 polytype ($W_{IIbb,y=0b}$ or W_{IIb-2}), (2) distribution of Fe between the 2:1 layer and the interlayer sheet (R_{int}), and (3) the percentage of layers shifted only in one direction, +1/3**b** or −1/3**b** ($W_{IIbb,y=+1/3b}$ or W_{IIb-4} and $W_{IIbb,y=−1/3b}$ or W_{IIb-6}), thus the proportion of IIb-4 and IIb-6 polytypes (R_{shift}), were introduced. All the above modifications

were considered for $R0$ (random interstratification) and $R1$ (interstratification described by W_j and P_{ij} probabilities with $W_j \neq P_{ij}$) types of stacking order. In addition, the interstratification of different polytypes was analyzed; thus, parameters describing the probability of finding Ibb, Iaa, Iab, Ibb, IIab, and IIaa polytypes fragments were added.

Separately, the possible disorders of the orientation of successive 2:1 layers with rotations by 0, 120, and 240° were considered along with three translations in y for each case (0, +1/3**b**, and –1/3**b**), which gives a structure with 9 types of layers. For both cases (polytypes and 2:1 layer rotations), only $R0$ ordering was assumed, which means that the P_{ij}—the probability of finding j-type layer after i-type layer in layers succession, was equal to W_j—the probability of the presence of a given polytype or rotated fragment in the structure: $P_{ij} = W_j$. Trigonal rotational axes perpendicular to the interlayer plane imposes that after rotation by 120 and 240°, it is indistinguishable from the original one. Therefore, only rotations of 2:1 layer were considered. In this model it was assumed that: $W_{rot=0} = W_{rot=120} = W_{rot=240}$, and $W_{rot=X,y=+1/3\mathbf{b}} = W_{rot=X,y=-1/3\mathbf{b}}$ (where X = 0, 120, 240°). The only optimized parameter was the percent of layers not shifted along **b**.

Also, the simulation of interstratification with 7 Å mineral was performed assuming only $R0$ ordering (Sybilla 2D). Detailed information about the parameters used in the individual calculations is given in Table 1.

Unit-cell parameters for all the samples were fitted using the Le Bail approach (Le Bail et al. 1988) implemented in Jana2006 software (Petricek et al. 2014). However, in three cases (MAL, CCa-2, and Mtbl) in which hkl reflections with $k \neq 3n$ were detectable, a conventional indexing procedure was also used.

RESULTS AND DISCUSSION

Chemical typology of the studied chlorites

The studied chlorites represent a uniform Mg-Fe series where the total Fe content ranges from 0.1 in clinochlore (POST) to 3.9 in chamosite (SG7) and the proportional Mg content ranges from 4.56 to 0.45 atoms per half formula unit (Table 2, Fig. 1) (Bayliss 1975; Guggenheim et al. 1996). All Si was assigned to the tetrahedral position and completed to four with Al; the remaining Al was assigned to the octahedral position along with Mg, Fe, Mn,

Cr, and Ni cations. To fill six octahedral positions, the number of vacancies were calculated; however, it cannot be ruled out that this is an artifact from the EMPA analytical error. No tetrahedral Fe was found using either Mössbauer spectroscopy or formula calculation in any of the studied samples.

General classification, admixtures, and the interstratification of 14 and 7 Å layers

Detailed analysis of XRD patterns obtained for disoriented specimens including full-width at half maximum (FWHM) (β) measurements of 00l reflections excludes the possibility of $R0$ interstratification of 14 and 7 Å layers (cf. Reynolds 1988; Reynolds et al. 1992; Drits et al. 2001; Inoue and Kogure 2016). A 00l peak width [$\beta \cdot \cos(\theta)$] vs. peak diffraction order for 001 to 005 is shown in Figure 2. As observed in all the studied samples, there is no tendency for line broadening of odd-order peaks (Fig. 2), which is typical for 7 Å-interstratified $R0$ chlorites (Reynolds et al. 1992). A slight increase in reflection width with 2θ is an expected outcome related to the strain effect and the $K\alpha_1$-$K\alpha_2$ separation (the calculation of FWHMs with stripped $K\alpha_2$ are presented in Supplemental[1] Fig. S1). To confirm our statement, the simulation assuming $R0$ interstratification of 14 and 7 Å layers was performed. The serpentinite d_{001} was assumed as 7.09 Å according to crystallographic data presented by Slack et al. (1992). Results show that even an assumption of 2% of 7 Å mineral interstratification significantly changed the calculated diffraction patterns leading to broadening of the odd number reflections. In Supplemental[1] Figure S2, the FWHM values for diffraction patterns simulated with 2, 5, 10, and 30% serpentinite layers content, are presented.

TABLE 1. Detailed information on the parameters used in the simulation

Parameter	Description
General parameters (parameters used in all simulations)	
Sigma star (SS) σ	Parameter describing degree of preferred orientation (Reynolds 1986)
N_{mean}	Mean number of crystallites along c* direction
Particle Radius (PR)*	Mean a×b plane radius
d	00l distance for chlorite
b	b unit-cell parameter
Fe$_{tot}$	Total Fe content per unit cell
Interlayer content (IC)	Octahedral sheet occupancy in the interlayer
R_{Fe}	Percentage of Fe in the interlayer relative to Total Fe content, $R_{Fe} = Fe_{int}/Fe_{tot}$
$W_{IIbb,y=0\mathbf{b}}$	Probability of occurrence of IIbb layers without a shift along **b** (IIb-2 content)
R_{shift}	Probability of finding the ⅓**b** shift in one direction
Simulation of 14 Å and 7 Å layer interstratification	
d	001 distance for serpentinite
SerR$_{Fe}$	Octahedral iron content in serpentinite
W_i	Probability of finding 7 Å layers
Simulation of polytype interstratification	
W_{IIbb}	Probability of occurrence of the IIbb polytype in the sample(y = 0**b**, +⅓**b**, −⅓**b**)
W_{Iaa}	Probability of occurrence of the Iaa polytype in crystals (y = 0**b**)
W_{Iab}	Probability of occurrence of the Iab polytype in crystals (y = 0**b**)
W_{Ibb}	Probability of occurrence of the Ibb polytype in crystals (y = 0**b**)
W_{IIab}	Probability of occurrence of the IIab polytypecrystals(y = 0**b**)
W_{IIaa}	Probability of occurrence of the IIaa polytype in crystals (y = 0**b**)
Simulation of rotations of 2:1 layer	
$W_{rot=0}$	Probability of occurrence of 2:1 layer rotated about 0°
$W_{rot=120}$	Probability of occurrence of 2:1 layer rotated about 120°
$W_{rot=240}$	Probability of occurrence of 2:1 layer rotated about 240°
$W_{rot=0,y=0\mathbf{b}}$	Probability of occurrence of layers rotated about 0° without a shift along **b**
$W_{rot=0,y=\pm1/3\mathbf{b}}$	Probability of occurrence of layers rotated about 0° with a shift along **b** = ±⅓**b**
$W_{rot=120,y=0\mathbf{b}}$	Probability of occurrence of layers rotated about 120° without a shift along **b**
$W_{rot=120,y=\pm1/3\mathbf{b}}$	Probability of occurrence of layers rotated about 120° with a shift along **b** = ±⅓**b**
$W_{rot=240,y=0\mathbf{b}}$	Probability of occurrence of layers rotated about 240° without a shift along **b**
$W_{rot=240,y=\pm1/3\mathbf{b}}$	Probability of occurrence oflayers rotated about 240° with a shift along **b** = ±⅓**b**
Simulation assuming $R1$ ordering	
P_{ij}	Junction probabilities of finding j-type of layer after i-type of layer (in the case of 3-layer type, there are 9 junction probabilities)

TABLE 2. Chemical compositions of chlorite samples

	POST	Mal	CCC	Sptb	CCa2	MtBl	SG7	Analytical techniques
SiO_2	30.77 ± 0.57	29.93 ± 0.33	30.23 ± 0.426	28.035 ± 0.205	26.42 ± 0.52	23.79 ± 0.25	23.31 ± 0.39	a
Al_2O_3	22.48 ± 1.00	20.75 ± 0.33	19.79 ± 0.493	20.39 ± 0.20	21.17 ± 0.76	20.49 ± 0.29	20.28 ± 0.56	a
FeO	1.38 ± 0.85	4.05 ± 0.45	5.495 ± 0.22	16.00 ± 0.24	20.656 ± 0.63	36.29 ± 0.52	39.60 ± 0.82	a,b
Fe_2O_3	0.03 ± 0.02	1.20 ± 0.045	1.62 ± 0.06	1.13 ± 0.17	2.00 ± 0.06	2.12 ± 0.03	2.81 ± 0.17	a,b
Cr_2O_3	b.d.l.	0.20 ± 0.02	0.13 ± 0.04	b.d.l.	0.04 ± 0.03	b.d.l.	b.d.l	a
MgO	33.25 ± 0.89	31.58 ± 0.40	31.01 ± 0.49	22.63 ± 0.24	18.52 ± 0.625	5.586 ± 0.16	2.70 ± 0.63	a
MnO	b.d.l.	b.d.l.	0.12 ± 0.04	0.12 ± 0.05	0.085 ± 0.045	0.822 ± 0.08	0.83 ± 0.21	a
NiO	b.d.l.	0.25 ± 0.03	0.13 ± 0.03	b.d.l.	0.09 ± 0.05	b.d.l.	b.d.l	a
TiO_2	0.02 ± 0.01	0.09 ± 0.01	0.05 ± 0.01	0.03 ± 0.01	0.07 ± 0.03	0.025 ± 0.01	0.03 ± 0.01	a
$H_2O(+)$	12.91	12.66	12.56	12.00	11.73	10.78	10.57	a
				Number of atoms per half formula unit				
Si	2.83 ± 0.04	2.810 ± 0.015	2.85 ± 0.03	2.79 ± 0.02	2.68 ± 0.05	2.64 ± 0.02	2.64 ± 0.03	
Al^{IV}	1.17 ± 0.11	1.190 ± 0.024	1.15 ± 0.05	1.21 ± 0.02	1.32 ± 0.09	1.35 ± 0.03	1.36 ± 0.06	
Al^{VI}	1.27 ± 0.11	1.105 ± 0.024	1.04 ± 0.05	1.17 ± 0.02	1.22 ± 0.09	1.33 ± 0.03	1.34 ± 0.06	
Cr^{3+}	b.d.l.	0.020 ± 0.003	0.010 ± 0.004	b.d.l.	b.d.l.	b.d.l.	b.d.l.	
Fe^{3+}	0.002 ± 0.001	0.085 ± 0.003	0.115 ± 0.005	0.085 ± 0.01	0.150 ± 0.005	0.18 ± 0.002	0.24 ± 0.02	
Fe^{2+}	0.11 ± 0.07	0.32 ± 0.013	0.43 ± 0.02	1.33 ± 0.02	1.755 ± 0.06	3.37 ± 0.04	3.75 ± 0.09	
Mg	4.56 ± 0.11	4.42 ± 0.04	4.35 ± 0.06	3.35 ± 0.03	2.80 ± 0.09	0.93 ± 0.03	0.45 ± 0.10	
Mn	b.d.l.	b.d.l.	0.010 ± 0.004	0.010 ± 0.004	0.007 ± 0.004	0.08 ± 0.007	0.08 ± 0.02	
Ni	b.d.l.	b.d.l.	0.010 ± 0.002	b.d.l.	0.007 ± 0.004	b.d.l.	b.d.l.	
Fe/(Fe+Mg)	0.02	0.08	0.11	0.30	0.405	0.79	0.90	
Total oct	5.94	5.95	5.965	5.945	5.94	5.89	5.86	

Notes: Analytical techniques: a = electron microprobe analysis, b = Mössbauer analysis. b.d.l. = below detection limit.

Based on powder diffraction patterns, all the studied samples may be classified as nearly pure trioctahedral IIb-even (IIbb) chlorites (Brown and Brindley 1962). Some of the samples contained small admixtures of other minerals—total below 3%: rutile in POST and quartz in Mal, CCC, Sptb, Mtbl, and SG7. In all the studied samples, semi-random stacking manifests itself as the decreased intensity of peaks in the region between 20 and 28° 2θ (CoKα) where 02*l* and 11*l* (1*l*) reflections are present. The diffraction patterns of the "end-members" in respect of Fe content of the studied chlorite series are shown in Figure 3. See Supplemental[1] Figure S3 for all other XRD patterns.

### Determination of unit-cell parameters: Chlorite indexing

In the XRD patterns of the studied chlorites, the observed first 20 low 2θ angle reflections belong to either 00*l* or *h*0*l* overlapping with *hkl* (*k* = 3*n*); thus, the calculation of unit-cell parameters is difficult due to the indeterminacy of the b dimension as well as α and γ angles. Nevertheless, for Mal, CCa-2, and Mtbl chlorites, in the range 20–28° 2θ (CoKα), *hkl* reflections with *k* ≠ 3*n* were slightly distinguishable (Supplemental[1] Fig. S4), which suggested better structural ordering, offering a chance for appropriate indexing. For all the above chlorites, the calculated unit-cell parameters (using TOPAS software) were close to expected for a monoclinic-shaped cell (β = 97°) and in two cases—CCa-2 and Mtbl—the α and γ angles were found to be 90° (Table 3). The indexing of the Mal sample resulted in a primitive (*L*) unit cell, thus the transformation into a *C*-centered cell was performed using the transformation matrix shown below:

$$\begin{bmatrix} a \\ b \\ c \end{bmatrix} \begin{bmatrix} 1 & \bar{1} & 0 \\ 1 & 1 & 0 \\ 0 & 0 & 1 \end{bmatrix} = \begin{bmatrix} a' \\ b' \\ c' \end{bmatrix}$$

As shown in Table 3, the obtained unit-cell shape is not perfectly monoclinic-like. The output sheets for these solutions are presented in the Supporting Information[1].

A structural model with a monoclinic-shaped cell and $C\bar{1}$ symmetry, as determined by Zanazzi et al. (2009), was used for Le Bail fitting. This choice was made considering the fact that IIb-4 is the polytype most frequently observed in nature in regular-stacking samples as well as based on the conclusion by Brown and Bailey (1962) that all chlorites with semi-random
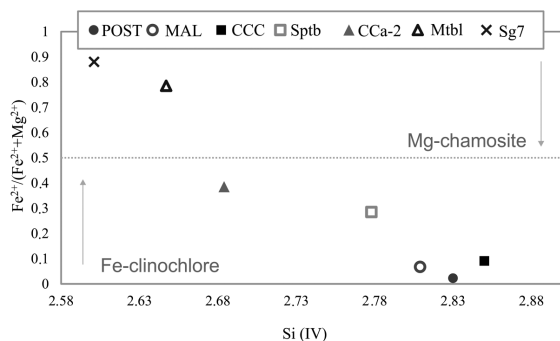
FIGURE 1. Compositions of natural chlorites used in our study projected onto the chemographic coordinates.
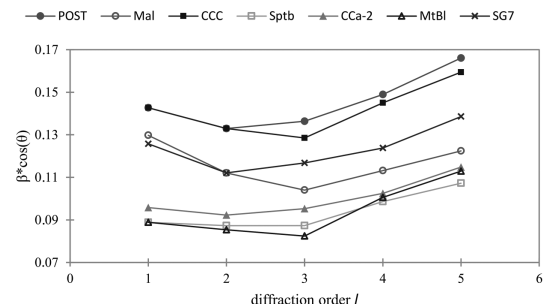
FIGURE 2. Calculated peak widths multiplied by cos(θ) for all investigated chlorites vs. diffraction order for the 001 to the 005 reflections for disoriented specimens. No removal of instrumental broadening effects or stripping of the *K*α₂ signal was performed.
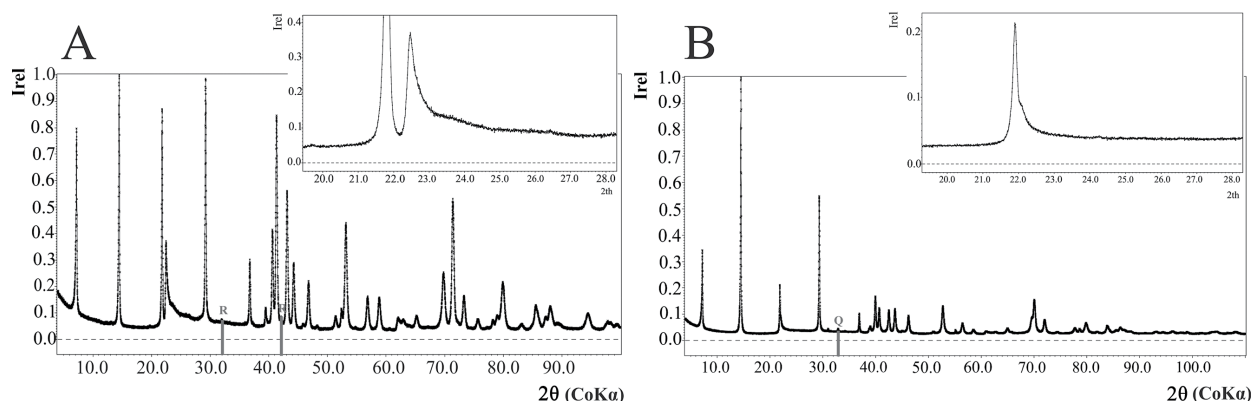
FIGURE 3. Diffraction patterns and their inserts with the region between 20 to 28° 2θ (CoKα) of (**a**) POST chlorite (low Fe content) and (**b**) SG7 chlorite (high Fe content). Note large differences in peak intensity in the inserts. The largest peaks corresponding to admixtures are shown using gray lines with letters: R = rutile, Q = quartz.

TABLE 3. Unit-cell parameters obtained from the indexing procedure implemented in TOPAS software

	Mal[a]	CCa-2	Mtbl
a (Å)	5.7073 (5.5667)	5.3568	5.3890
b (Å)	5.3263 (9.4730)	9.2688	9.3371
c (Å)	14.2559 (14.2560)	14.2608	14.2441
α (°)	86.4920 (89.50)	90.0000	90.0000
β (°)	92.4370 (95.76)	97.0550	97.3640
γ (°)	61.7230 (85.51)	90.0000	90.0000
V (Å³)	379.670 (759.24)	702.701	710.817
GOF[b] (%)	14.16	18.53	31.70

[a] The cell parameters in C-centered cell are present in the partentheses.

[b] GOF $= \sqrt{\frac{w(y_o - y_c)^2}{M - L}}$, $w = 1/(y_o)$, y_o is observed intensity, y_c is calculated intensity, M is the number of data points, L is number of parameters.

stacking should have triclinic symmetry as a result of averaging of two potential triclinic and one monoclinic layer symmetries. In the three chlorites analyzed, the background, zero shift, unit cell, and profile parameters including asymmetry were fitted simultaneously. As expected, *hkl* reflections with $k \neq 3n$ were not fitted to a satisfying level; however, this lack of proper fit may be accepted since its impact on the determination of unit-cell parameters was negligible. Calculated cell parameters are provided in Table 4. The known dependency, $a = b/\sqrt{3}$, is preserved for calculated parameters.

The obtained results, from both the conventional indexing and Le Bail fitting, can be considered as equally reliable, as long as no conclusion about symmetry is drawn based on these results.

Layer stacking disorder considering $R0$ ordering

In the three studied samples, where *hkl* reflections with $k \neq 3n$ were distinguishable, suggesting a higher ordering of these structures, their stacking pattern could be determined based on XRD features in the range 20–28° 2θ (CoKα). Therefore, by a comparison between experimental and simulated diffraction patterns, the semi-random stacking sequence can be identified (cf. Kogure et al. 2006; Kameda et al. 2007).

Sets of parameters provided in Table 1 were optimized using Sybilla3D software according to two different protocols (Protocols S1, S2) and assuming $R0$ ordering, as shown in Table 5. In all performed simulations, the total Fe content and the percentage of vacancies were fixed based on chemical compositions (Table 2).

The vacancies were assumed to be present only in the interlayer sheet, for the sake of simplification. The σ star parameter was optimized to reflect increasing crystallite orientation in Fe-rich chlorite specimens.

In the first step of each simulation (Protocol S1, Table 5), all the parameters excluding the total Fe content and percentage of vacancies were fitted simultaneously. The obtained b and **c*** parameter values were in good agreement with those obtained using Le Bail fitting (comparison in Supplemental[1] Table S1 in the electronic appendix). In the Supplemental[1] Table S1 protocol, the percentage of layers shifted at $-\frac{1}{3}\mathbf{b}$ was assumed to be equal to that shifted about $+\frac{1}{3}\mathbf{b}$; thus the R_{shift} was fixed at 0.5 ($W_{IIb-4} = W_{IIb-6}$). Several simulated XRD patterns for different values of $W_{IIbb,y=0b}$, thus different IIb-2 content, are shown in Figure 4 for two chlorites with different shapes of the diffraction pattern in the range 20–28° 2θ (CoKα) and different Fe contents. Simulations for all other samples are shown in Supplemental[1] Figures S5–S9.
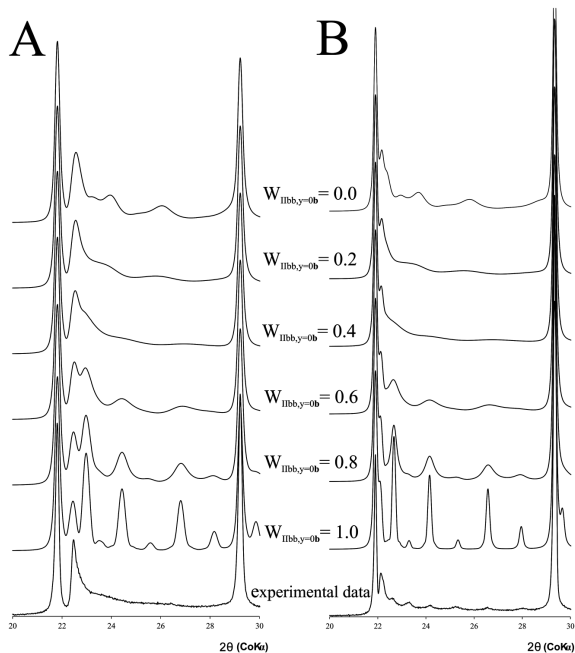
In all the studied chlorites, the distribution of Fe between the interlayer sheet and 2:1 layer had a strong impact on simulated XRD patterns. The modeled crystallite orientation (σ star parameter) strongly correlated with the results of Fe distribution. The general tendency found as a result of the simulations indicates that in clinochlorites, Fe occurs mostly in the interlayer sheet; with increasing Fe content, the distribution between the octahedral sheets of the interlayer and the 2:1 layer becomes uniform (close to 50:50).

As observed in Protocol S1 results, the change in the $W_{IIbb,y=0b}$ parameter (with the assumption that $R_{shift} = 0.5$, thus $W_{IIb-4} = W_{IIb-6}$) has a significant impact on the diffraction patterns in the range 20–28° 2θ, offering an opportunity to investigate disordered layer stacking in chlorites. In four cases: POST, CCC, Sptb, and SG7, $W_{IIbb,y=0b}$ was found to be between 0.2 and 0.4, indicating that 20 to 40% of the layers are not shifted at ±1/3**b**. In turn, in three other cases (Mal, CCa-2, Mtbl), this simple approach turned out to be insufficient for obtaining a good fit (Supplemental[1] Figs. S5, S8, and Fig. 4b, respectively).

In the second step (Protocol S2, Table 5), the fit parameter values obtained in step S1 were used as inputs along with the parameter expressed as the percentage of layers shifted only in one direction (R_{shift}), +1/3**b** or −1/3**b**. In the case of POST, CCC,

Sptb, and SG7 chlorites, no significant improvements of fit were found, mostly due to the fact that R_{shift} had changed slightly in comparison to the value 0.5 fixed in Protocol S1, and optimized values were in the range 0.5–0.6. However, using the S2 simulation protocol for CCa-2 and Mtbl, the obtained fit was better than that using the S1 protocol, but still not perfect (Figs. 5a and 5b, respectively). Nevertheless, the results showed that in these two cases, roughly 80 to 90% of layers were shifted in one direction (R_{shift} = 0.8–0.9), suggesting some kind of ordering manifested in a one-direction shift of layers in the **b** crystallographic direction (predominance of one polytype IIb-4 or IIb-6). During the S2 simulation, the input parameters obtained from S1 were refined; however, the values remained essentially identical.

Due to the persistently poor fit of CCa-2 and Mtbl patterns, the presence of an additional, highly ordered chlorite phase was postulated: the $W_{IIbb,y=0b}$ and R_{shift} parameters for these additional structures were refined and yielded 0.7 and 0.8, respectively. Other parameters were fixed at the same values as in the dominant chlorite phase (details in Supplemental[1] Table S2). This approach led to a significant improvement of fit, which is clearly visible in Figure 6.

In summary, in the case of CCa-2 and Mtbl (assuming $R0$ ordering), two effects are responsible for the unique features of XRD patterns in the range 20–28° 2θ (Fig. 6). The first effect is related to a preferential shift along **b** in one direction (predominance of IIb-4 or IIb-6), and the second effect was due to the presence of an additional, highly ordered phase, where almost 70% of the layers are not shifted along **b** (predominance of IIb-2). We emphasize that the presence of both these phases is required to obtain an acceptable fit for $R0$ ordering.

In the case of chlorite Mal, assuming only the presence of a second, highly ordered chlorite population was insufficient to obtain a good fit. To obtain a matching simulation, an assumption of the presence of three phases was required, including one with a much lower value of the b parameter (Fig. 7). The presence of three phases may explain difficulties with the indexing and obtaining of a deformed unit cell for the chlorite Mal (Table 3). Details of the optimization for chlorite Mal are presented in the Supplemental[1] Table S3.
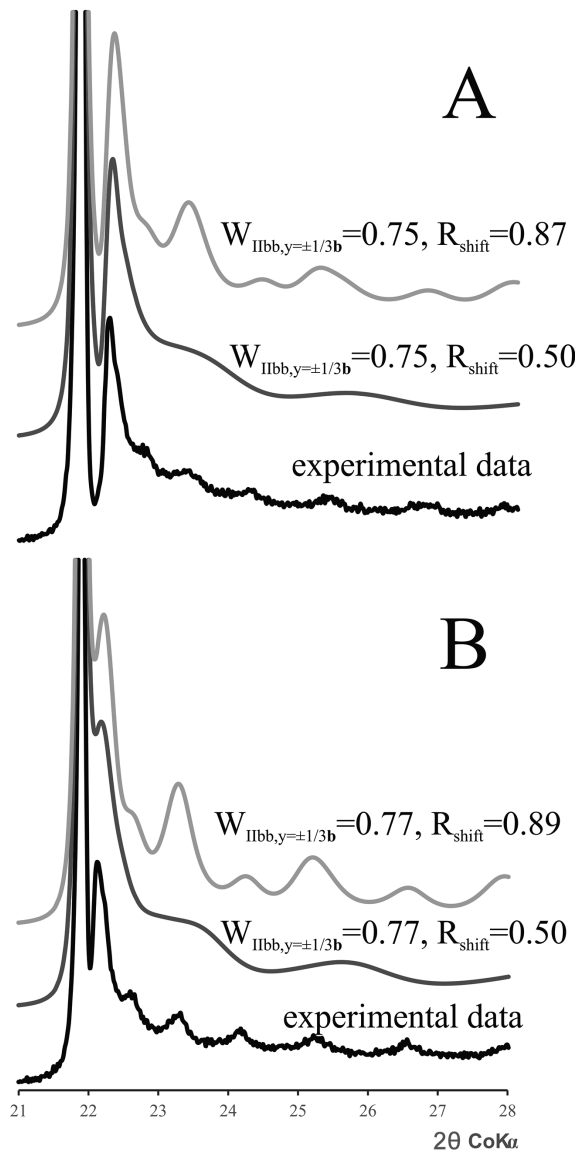
Interstratification of different polytypes assuming $R0$ ordering

Because different polytypes (Supplemental[1] Fig. S10) can occur not only as different crystallite populations, but also as part of a stacking sequence, parameters describing the interstratification of different polytypes were also considered during the

FIGURE 4. Comparison of experimental and simulated XRD patterns of semi random-stacking chlorites in the range 20–30° 2θ for (**a**) POST chlorite (low Fe content) and (**b**) Mtbl chlorite (high Fe content). $W_{IIbb,y=0b}$ was calculated assuming that the number of layers shifted by +1/3**b** is equal to the number of layers shifted by –1/3**b**, i.e., R_{shift} = 0.5.

TABLE 5. Parameters that were fixed and optimized in the applied calculation protocols using modified Sybilla 3D code

Parameter	Protocol S1	Protocol S2	Protocol S3	Protocol S4	Protocol S5
Sigma star (SS) σ*	refined	refined	refined	fixed	fixed
N_{mean}	refined	refined	refined	fixed	fixed
Particle Radius (PR)	refined	refined	refined	fixed	fixed
d	refined	refined	refined	fixed	fixed
b	refined	refined	refined	fixed	fixed
Fe_{tot}	fixed	fixed	fixed	fixed	fixed
Interlayer content (IC)	fixed	fixed	fixed	fixed	fixed
R_{Fe}	refined	refined	refined	fixed	fixed
W_{IIbb}	Fixed = 1	Fixed = 1	refined	Fixed = 1	Fixed = 1
$W_{IIbb,y=0b}$	refined	refined	refined	–	fixed
R_{shift}	Fixed = 0.5	refined	refined	Fixed = 0.5	fixed
W_{Iaa}	Fixed = 0	Fixed = 0	refined	–	Fixed = 0
W_{Iab}	Fixed = 0	Fixed = 0	refined	–	Fixed = 0
W_{Ibb}	Fixed = 0	Fixed = 0	refined	–	Fixed = 0
W_{IIab}	Fixed = 0	Fixed = 0	refined	–	Fixed = 0
W_{IIaa}	Fixed = 0	Fixed = 0	refined	–	Fixed = 0
$W_{rot=0}$	–	–	–	refined	–
$W_{rot=120}$	–	–	–	refined	–
$W_{rot=240}$	–	–	–	refined	–
$W_{rot=0, y=0b}$	–	–	–	refined	–
$W_{rot=0, y=±1/3b}$	–	–	–	refined	–
$W_{rot=120, y=0b}$	–	–	–	refined	–
$W_{rot=120, y=±1/3b}$	–	–	–	refined	–
$W_{rot=240, y=0b}$	–	–	–	refined	–
$W_{rot=240, y=±1/3b}$	–	–	–	refined	–
P_{ij}	–	–	–	–	refined

Note: All abbreviations as in Table 1.

TABLE 4. Unit-cell parameters calculated using Le Bail fitting

	POST	Mal	CCC	Sptb	CCa-2	Mtbl	SG7
a (Å)	5.31209(12)	5.32801(19)	5.3318(2)	5.34355(17)	5.35619(13)	5.38984(13)	5.3968(5)
b (Å)	9.1997(3)	9.2271(5)	9.2327(5)	9.2577(2)	9.2766(3)	9.3344(3)	9.3508(10)
c (Å)	14.3017(3)	14.3023(6)	14.3090(9)	14.26647(16)	14.2615(4)	14.2387(3)	14.2349(5)
α (°)	90.955(4)	90.277(14)	90.540(13)	89.940(3)	90.393(3)	90.371(3)	90.687(13)
β (°)	97.157(2)	97.162(5)	97.124(4)	96.909(3)	97.234(2)	97.243(2)	97.294(8)
γ (°)	90.458(5)	89.448(11)	90.110(13)	90.122(3)	90.005(3)	89.990(3)	89.945(11)
V (Å³)	693.34(3)	697.61(5)	698.92(7)	700.62(3)	703.08(3)	710.48(4)	712.49(11)

FIGURE 5. Experimental and simulated data for (**a**) CCa-2 and (**b**) Mtbl for fits where R_{shift} was fixed at the value of 0.5 (dark gray line) and R_{shift} was refined ($W_{IIbb,y=\pm1/3b} = 1 - W_{IIbb,y=0b}$, light gray line).

third step of refinement (Protocol S3, Table 5). In an analogy to the previous step, the output parameters from step S2 were used as the inputs in S3. To limit the complexity of the model, besides IIbb, for which probabilities of all shifts along **b** were considered (0, ±1/3**b**), all the other polytypes' structures were refined, assuming that the shift along **b** equals zero. As it turned out, adding interstratification had only a minor impact on the range 20–28° 2θ; however, in the range 30–60° 2θ, a significant improvement of fit was observed (Fig. 8, Supplemental[1] Figs. S11–S16). The interstratification of polytypes other than IIbb (Iaa, IIab, and IIaa) was found in all the studied chlorite samples. The obtained fractions of other, interstratified polytypes ranged from 5 to 19% and were not correlated with Fe content in the samples. Similar results were observed by Kogure and Banfield

(1998); Inoue and Kogure (2016) used HRTEM to show the presence of several chlorite polytypic sequences including IIab, Iab, Ibb, and Iaa. In contrast to these studies, the IIaa phase was also found among the stacking sequences of the studied chlorite samples (Supplemental[1] Table S4). Fits in full 2θ range are presented in Supplemental[1] Figure S17–S23A.

Layer stacking disorder considering rotations of 2:1 layer assuming *R*0 ordering

The possible rotations of 2:1 layers by 0, 120, and 240° together with shifts along **b** (0, +1/3**b**, and –1/3**b**) were considered, giving nine types of layers (Protocol S4, Table 5). Results show that, the following structures turned out to be nearly equivalent: (1) (rot0, y = 1/3**b**) ≡ (rot0, y = –1/3**b**) ≡ (rot120, y = 0**b**) ≡ (rot 120, y = –1/3**b**) ≡ (rot240, y = 0**b**) ≡ (rot 240, y = +1/3**b**) (2) (rot0, y = 0**b**) ≡ (rot120, y = 1/3**b**) ≡ (rot240, y = –1/3**b**). The reason for this similarity for IIbb chlorite is presented in Supplemental[1] Fig. S24–S27.

In spite of this correspondence and thus very similar XRD patterns of structures in each of the two groups, stacking faults give different results for rotation defects and structures with shifts along **b** (Fig. 9). In the case of the structure containing
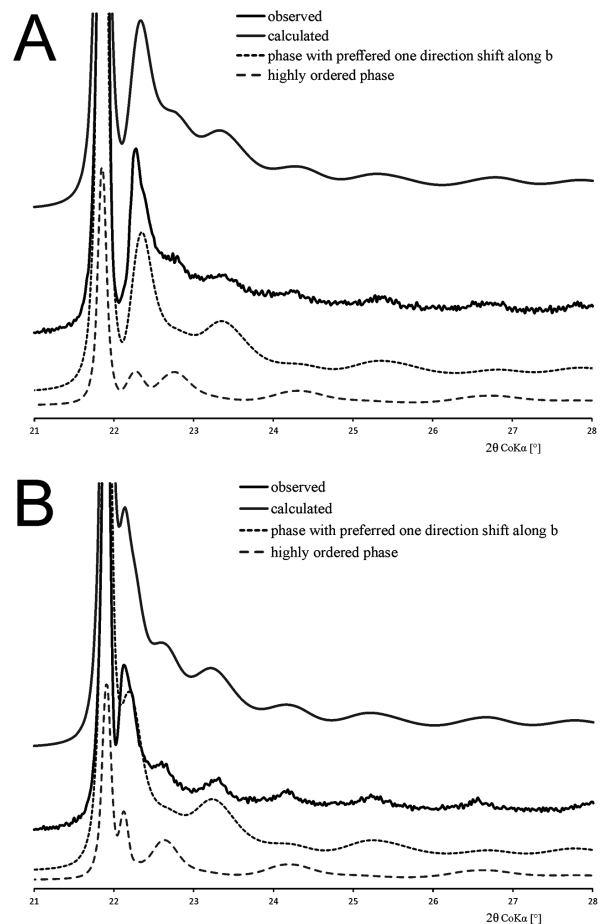
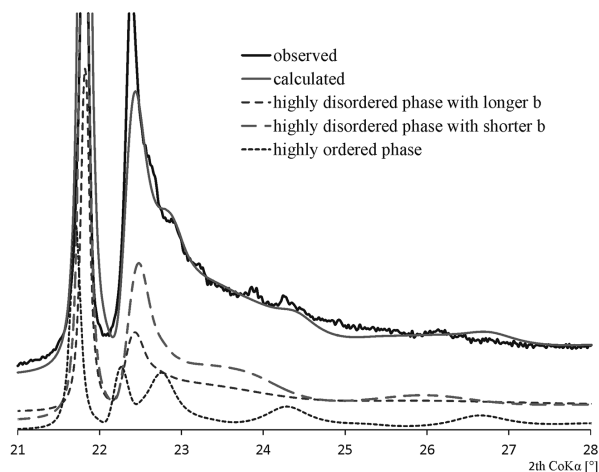**FIGURE 6.** Experimental and simulated data for (**a**) CCa-2 and (**b**) Mtbl for models considering two chlorite phases.

FIGURE 7. Experimental and simulated data for Mal assuming the presence of three phases.

FIGURE 8. Comparison of fits for Mtbl models (**a**) without and (**b**) with consideration of interstratified polytypes other than IIbb. The error of calculation of probability was evaluated as ±2%.

only rotations in crystallite, there are seven well-separated peaks in the range 20–28° 2θ corresponding to *hkl* reflections with *k ≠ 3n*. Relative proportions between intensities of these peaks depend on proportions between rot0, y = 0**b**, rot120, y = 0**b**, and rot240, y = 0**b**. There is no significant broadening of reflections in the mixed layer crystallite. On the other hand, in the case of a crystallite composed of layers with shifts along **b**, peak broadening of *hkl* reflections with *k ≠ 3n* is significantly more pronounced (Fig. 9).

Calculated diffraction patterns for mixed layer structures that consider rotations and shifts along **b** have very good correspondence with experimental patterns of chlorites that have distinguishable *hkl* reflections with *k ≠ 3n*: CCa-2 and Mtbl (Fig. 10). In both cases, the best fits were obtained for equal content of 2:1 rotations ($W_{rot0} = W_{rot120} = W_{rot240} = 0.3333$). For each 2:1 rotation, R_{shift} was set as 0.5 ($W_{rot=X,y=+1/3\mathbf{b}} = W_{rot=X,y=-1/3\mathbf{b}}$; where: X = 0°, 120°, 240°) and the percent of layer not shifted along **b** (sum of $W_{rot=0,y=0\mathbf{b}}$, $W_{rot=120,y=0\mathbf{b}}$, and $W_{rot=240,y=0\mathbf{b}}$) was established as 75% and 64%, respectively, for Mtbl and CCa-2 (Supplemental[1] Table S5).

Layer stacking disorder considering *R*1 ordering

The output parameters from the protocol S2 were used as the input data for the simulation assuming *R*1 ordering. All parameters were fixed (the values obtained from S2), and only the junction probabilities of the stacking sequences were refined (protocol S5, Table 5). In the first step, the probability $P_{IIb-2\ IIb-2}$ was optimized. As it turned out, for chlorites POST, CCC, Sptb, and SG7, the best results were obtained, when the $P_{IIb-2\ IIb-2} = W_{IIb-2}$ (thus $P_{IIb-2\ IIb-2}$ is equal to the content of IIb-2). This result is identical to those obtained previously for *R*0 ordering. In turn, for chlorites CCa-2 and Mtbl, to obtain a reliable fit (Fig. 11), the $P_{IIb-2\ IIb-2}$ was evaluated as 0.5, thus higher than for *R*0 ordering ($W_{IIb-2} = 0.25$ and 0.23, respectively). All parameters are presented in Supplemental[1] Table S6.

This suggests some kind of segregation and presence in the structure domain with predominance of IIb-2 and IIb-4/-6 polytypes. It should be highlighted that this result does not contradict the fits with assumed *R*0 ordering. In this case, two populations
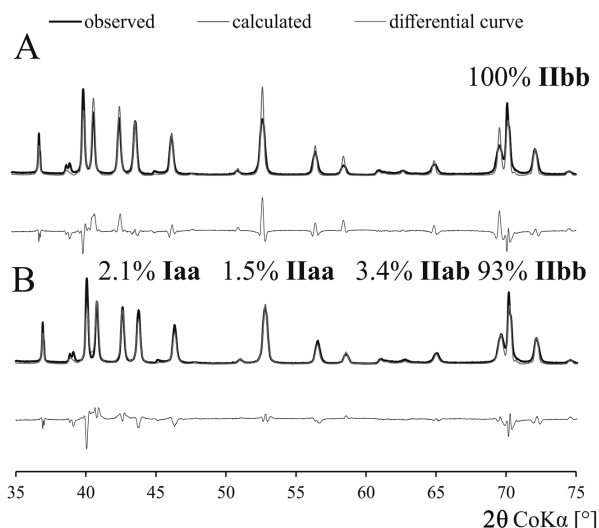
of chlorites that differ in content of IIb-2 and IIb-4 or IIb-6 was assumed to obtain satisfactory fits, which is also a kind of segregation. Fits are presented in Supplemental[1] Figure S17-23B.

Obtaining reliable fits for MAL was impossible since the presence of an additional phase with a lower d_{010} was probably needed, and in the case of *R*1 ordering, the model became too complicated.

Selection of the most probable model

There are several structural models that offer good agreement between experimental and calculated patterns of the studied chlorites for *hkl* reflections with *k ≠ 3n*:

- Assumption of more than one chlorite phases and shifts only along **b** (Figs. 6 and 7),
- Consideration of rotations and shifts along **b** (Figs. 9 and 10),
- Consideration of *R*1 ordering and shifts only along **b** (Fig. 11).

The second model is the most elegant as it contains the lowest number of parameters to be optimized. In the case of several phases in the system, there are many more parameters to be optimized and therefore there is a possibility to optimize a larger variability of experimental patterns, if assuming contrasting patterns as components. On the other hand, the third model (with *R*1 ordering) does not have an intuitive explanation for why certain P_{ij} parameters were chosen. Ordering for certain shift along **b** can, however, corresponds to some extent to the rotation, which was shown in Supplementary Materials[1]. Therefore, the second model can be chosen as the most probable. Moreover, this conclusion can be supported by HRTEM results as rotations by 120 and 240° were experimentally found (Kogure et al. 2017).
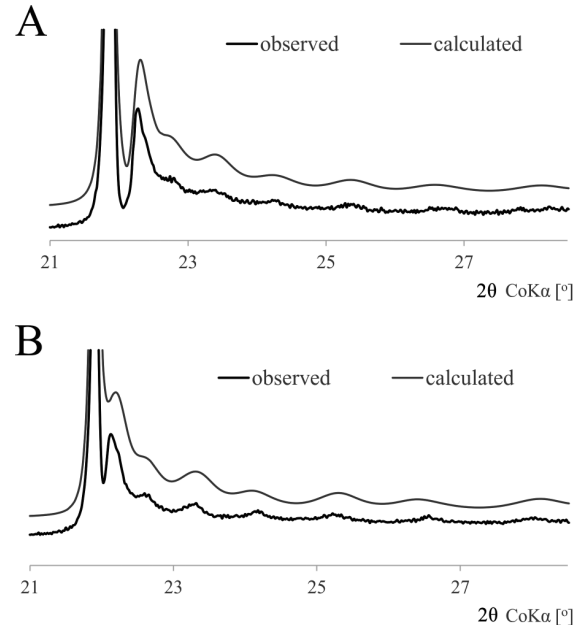
IMPLICATIONS

Chlorite polytypes are conventionally interpreted in terms of geothermometry for diagenesis, metamorphism, and

► **FIGURE 9.** Comparison of experimental and simulated XRD patterns for Mtbl chlorite in the range 20–28° 2θ, considering various percentages of different rotations and shifts along **b**.
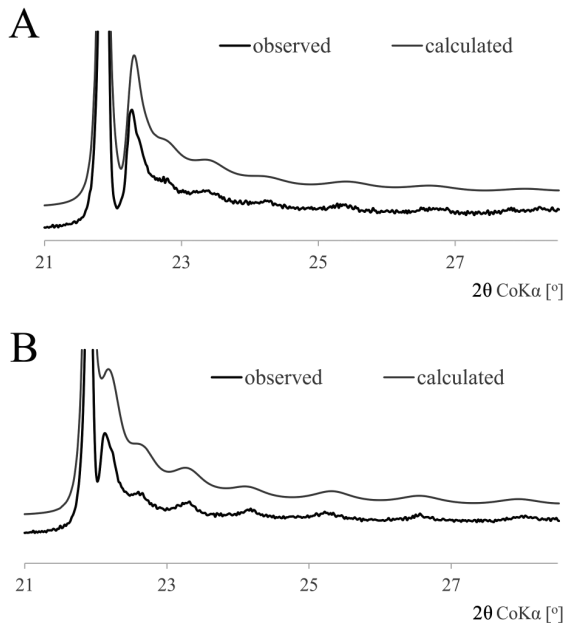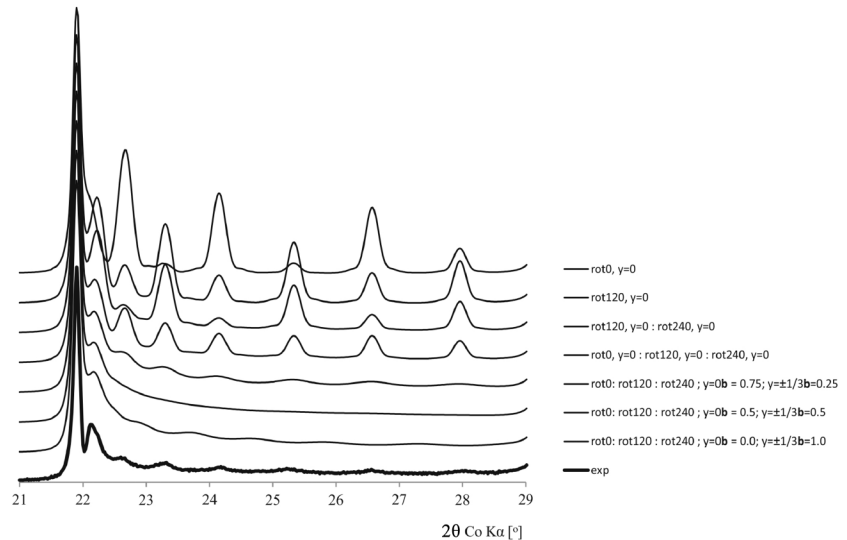
FIGURE 10. Experimental and simulated data for (**a**) CCa-2 and (**b**) Mtbl for models considering rotations of 2:1 layer and shifts along **b**.

FIGURE 11. Experimental and simulated data for (**a**) CCa-2 and (**b**) Mtbl assuming *R*1 ordering.

hydrothermal conditions (Walker 1993; Spoetl et al. 1994; Beaufort et al. 2015). In this study, we have shown how a careful simulation of chlorite powder X-ray diffraction (XRD) patterns allows for a comprehensive determination of the layers' stacking sequence with a combination of shifts not only in the crystallographic a direction (= conventional chlorite polytypism) but also in the **b** direction, which also significantly improves the interpretation of *hkl* reflections with $k \neq 3n$. Even in semi-random stacking chlorites, there is a certain kind of ordering manifesting itself as a predominant shift in one of the ±1/3**b** directions. The new capability of refining both dimensions of the chlorite stacking sequence—using common XRD

methods—offers new interpretations of chlorite formation conditions (cf. Mata et al. 2004).

Up to now, information about chlorite polytype interstratification was obtained mostly using high-resolution transmission electron microscopy (HRTEM) methodology on selected spots (Kogure and Banfield 1998; Mata et al. 2004; Inoue and Kogure 2016), but not on bulk samples. Powder XRD-based determination of polytype interstratification allows for the examination of chlorite polytype geothermometry as a continuous temperature-structure relationship, rather than thermal stability ranges of discrete polytypes (Walker 1993; Spoetl et al. 1994; Mata et al. 2004).

REFERENCES CITED

Ahn, H.J., and Peacor, D.R. (1985) Transmission electron microscope study of diagenetic chlorite in Gulf Coast argillaceous sediments. Clays and Clay Minerals, 33, 228–236.

Aja, S., Omotoso, O., Bertoldi, C., Dasch, E., and Benisek, A. (2015) The structure and thermochemistry of three Fe-Mg chlorites. Clay and Clay Minerals, 63, 351–367.

Bailey, S.W. (1986) Re-evaluation of ordering and local charge balance in Ia chlorite. Canadian Mineralogist, 24, 649–654.

Bayliss, P. (1975) Nomenclature of the trioctahedral chlorites. Canadian Mineralogist, 13, 178–180.

Beaufort, D., Rigault, C., Billon, S., Billault, V., Inoue, A., Inoue, S., and Patrier, P. (2015) Chlorite and chloritization processes through mixed-layer mineral series in low-temperature geological systems—a review. Clay Minerals, 50(4), 497–523.

Brindley, G.W., Oughton, B.M., and Robinson, K. (1950) Polymorphism of the chlorite. I. ordered structures. Acta Crystallographica, 3, 408–416.

Brown, B.E., and Bailey, S.W. (1962) Chlorite polytypism: 1. Regular and semi-random 1 layer structures. American Mineralogist, 47, 819–850.

Coelho, A.A. (2003) Indexing of powder diffraction patterns by iterative use of singular value decomposition, Applied Crystallography, 36, 85–96.

Drits, V.A., Ivanovskaya, T.A., Sakharov, B.A., Gor'kova, N.V., Karpova, G.V., and Pokrovskaya, E.V. (2001) Pseudomorphous replacement of globular glauconite by mixed-layer chlorite–berthierine in the outer contact of dike: Evidence from the Lower Riphean Ust'-Il'ya Formation, Anabar Uplift. Lithology and Mineral Resources, 36, 337.

Guggenheim, S., and Zhan, W. (1999) Crystal structures of three partially dehydrated chlorites: The 'modified' chlorite structure. American Mineralogist, 84, 1415–1421.

Guggenheim, S., Alietti, A., Bain, D.C., Drits, V.A., Formoso, M.M.L., Galan, E., Hudnall, W., Köster, H.M., Paquet, H., and Watanabe, T. (1997) Report of the Association Internationale pour l'Etude des Argiles (AIPEA) Nomenclature Committee for Clay Minerals, 32, 493–495.

Grazulis, S., Chateigner, D., Downs, R.T., Yokochi, A.T., Quirós, M., Lutterotti, L., Manakova, E., Butkus, J., Moeck, P., and Le Bail, A. (2009) Crystallography Open Database—an open-access collection of crystal structures. Journal of Applied Crystallography, 42, 726–729.

Herbillion, A., and Makumbi, M. (1975) Weathering of chlorite in a soil delivered from a chloritoschist under humid tropical conditions. Geoderma, 13, 89–104.

Hillier, S., and Velde, B. (1997) Octahedral occupancy and the chemical-composition of diagenetic (low-temperature) chlorites. Clay Mineralogy, 26(2), 149–168.

Inoue, S., and Kogure, T. (2016) High resolution transmission electron microscopy (HRTEM) study of stacking irregularity in Fe-rich chlorite from selected hydrothermal ore deposits. Clay and Clay Minerals, 64, 131–144.

Joswig, W., Fuess, H., Rothbauer, R., Takeuchi, Y., and Mason, S.A. (1980) A neutron diffraction study of a one-layer triclinic chlorite (penninite). American Mineralogist, 65, 349–352.

Kameda, J., Miyawaki, R., Kitagawa, R., and Kogure, T. (2007) XRD and HRTEM analyses of stacking structures in sudoite, di-trioctahedral chlorite. American Mineralogist, 92, 1586–1592.

Kogure, T., and Banfield, J.F. (1998) Direct identification of the six polytypes of chlorite characterized by semi-random stacking. American Mineralogist, 83, 925–930.

Kogure, T., Kameda, J., Matsui, T., and Miyawaki, R. (2006) Stacking structure in disordered talc: Interpretation of its X-ray diffraction pattern by using pattern simulation and high-resolution transmission electron microscopy. American Mineralogist, 91, 1363–1370.

Kogure, T., Ishii, T., Kikuchi, R., Miyawaki, R., and Yuguchi, T. (2017) Two types of chlorite transformed from biotite by hydrothermal alteration of granite. 16th International Clay Conference (Granada, Spain, July 20, 2017), 418.

Le Bail, A., Duroy, H., and Fourquet, J.L. (1988) Ab-initio structure determina-

tion of LiSbWO₆ by X-ray powder diffraction. Materials Research Bulletin, 23, 447–452.

Lempart, M., Derkowski, A., Luberda-Durnaś, K., Błachowski, A., and Skiba, M. (2018) Dehydrogenation and dehydroxylation as drivers of the thermal decomposition of Fe-chlorites. American Mineralogist, 103, 1837–1850.

Mata, M.P., Peacor, D.R., and López-Aguayo, F. (2004) Polytypism of cookeite in low-grade metapelites of the Cameros Basin, Spain: Lack of correlation of well-ordered polytypes with pressure. American Mineralogist, 89, 1510–1515.

Pauling, L. (1930) The structure of the chlorites. Proceedings of the National Academy of Sciences, 16, 578–582.

Petricek, V., Dusek, M., and Palatinus, L. (2014) Crystallographic Computing System Jana2006: general features. Zeitschrift für Kristallographie, 229(5), 345–352.

Post, J., and Plummer, C. (1972) The chlorite series of Flagstaff Hill area, California: A preliminary investigation. Clays and Clay Minerals, 20, 271–283.

Reynolds, R.C. (1986) The Lorenz-Polarization factor and preferred orientation in oriented clay aggregates. Clays and Clay Minerals, 34, 359–367.

——— (1988) Mixed layer chlorite minerals. In S.W. Bailey, Ed., Hydrous Phyllosilicates Exclusive of Micas, 19, p. 601–629. Reviews in Mineralogy, Mineralogical Society of America, Chantilly, Virginia.

Reynolds, R.C. Jr., DiStefano, M.P., and Lahann, R.W. (1992) Randomly inter-stratified serpentine/chlorite: its detection and quantification by powder X-ray diffraction methods. Clays and Clay Minerals, 40, 262–267.

Ryan, P.C., and Reynolds, R.C. Jr. (1996) The origin and diagenesis of grain-coating serpentine-chlorite in Tuscaloosa formation sandstone. American Mineralogist, 81, 213–225.

Shirozu, H., and Bailey, S.W. (1965) Chlorite polytypism. III. Crystal structure of an orthohexagonal iron chlorite. American Mineralogist, 50, 868–885.

Slack, J.F., Jiang, W.-T., Peacor, D.R., and Okita, P.M. (1992) Hydrothermal and metamorphic berthierine from the Kidd Kreek volcanogenic massive sulfide deposit, Timmins, Ontario. Canadian Mineralogist, 30, 1127–1142.

Spoetl, C., Houseknecht, D.W., and Longstaffe, F.J. (1994) Authigenic chlorites in sandstones as indicators of high-temperature diagenesis, Arkoma foreland basin, USA. Journal of Sedimentary Research, 64(3a), pp. 553–566.

Walker, J.R. (1993) Chlorite polytype geothermometry. Clays and Clay Minerals, 41(2), 260–267.

Walker, J.R., and Bish, D.L. (1992) Application of Rietveld refinement techniques to a disordered IIb Mg-chamosite. Clays and Clay Minerals, 40, 319–322.

Welch, M.D., and Marshall, W.G. (2001) High-pressure behavior of clinochlore. American Mineralogist, 86, 1380–1386.

Zanazzi, P.F., Montagnoli, M., Nazzareni, S., and Comodi, P. (2006) Structural effects of pressure on triclinic chlorite: A single-crystal study. American Mineralogist, 91, 1871–1878.

Zanazzi, P.F., Montagnoli, M., Nazzareni, S., and Comodi, P. (2007) Structural effects of pressure on monoclinic chlorite: A single-crystal study. American Mineralogist, 92, 655–661.

Zanazzi, P.F., Comodi, P., Nazzareni, S., and Andreozzi, G.B. (2009) Thermal behaviour of chlorite: an in situ single-crystal and powder diffraction study. European Journal of Mineralogy, 21, 581–589.

Zheng, H., and Bailey, S.W. (1989) Structures of intergrown triclinic and monoclinic IIb chlorites from Kenya. Clays and Clay Minerals, 37, 308–316.

Xu, H., and Veblen, D.R. (1996) Interstratification and other reaction micro-structures in the chlorite-berthierine series. Contributions to Mineralogy and Petrology, 124, 291–301.

Endnote:

[1]Deposit item AM-20-36982, Supplemental Material. Deposit items are free to all readers and found on the MSA website, via the specific issue's Table of Contents (go to http://www.minsocam.org/MSA/AmMin/TOC/2020/Mar2020_data/Mar2020_data.html).